Explore what's possible with innovative research tools

Attaining high-dimensional scientific insights can be overwhelming but with BD you're never alone.

Built on over 45 years of flow cytometry expertise, our line of innovative research tools and services offers you a complete cell analysis solution to streamline your research and support you on the path to experimental success. Our advanced flow cytometers, informatics and reagents combined with multiomics instrumentation can help you harness the power of high-dimensional biology to rapidly expand your understanding of complex biological systems.

So, go beyond your research limitations and explore with confidence. Discover the difference.

bdbiosciences.com/expand

BD

Cytometry PART A
Journal of Quantitative Cell Science

MIFlowCyt

A Novel Flow Cytometry Tool for Fibrosis Scoring Through Hepatic Stellate Cell Differentiation

Johnny Amer,* Ahmad Salhab, Sarit Doron, Gilles Morali, Rifaat Safadi

Liver and Gastroenterology Units, Hadassah University Medical Center, Jerusalem, Israel

Received 3 March 2017; Revised 15 May 2017; Accepted 19 August 2017

Additional Supporting Information may be found in the online version of this article.

*Correspondence to: Johnny Amer, PhD, Liver & Gastroenterology Units, Hadassah University Medical Center, POB 12000, Jerusalem 91120, Israel.
E-mail: johnnyamer@hotmail.com

Published online 8 March 2018 in Wiley Online Library (wileyonlinelibrary.com)

DOI: 10.1002/cyto.a.23202

Abstract

Hepatic stellate cells (HSCs) are a central fibrogenic cell type that contributes to collagen accumulation during chronic liver disease. Peripheral blood lymphocytes from HCV patients are phagocytized by HSCs and induce their differentiation. This study aimed to characterize HSCs differentiation using a flow cytometry tool for fibrosis scoring. NK cells from healthy donors and from patients with chronic HCV with various severities of fibrosis were co-cultured with a human HSC line (LX2). LX2 phagocytosis of NK cells were stained for NK cells (CD45/CD56/CD3) and NK activation marker (CD107a) as well as INF-γ, apoptosis (Annexin-V) and α-smooth-muscle-actin (αSMA, as a marker of LX2 activation). In addition, reactive oxygen species (ROS) and the senescence marker P15 were analyzed prior to flow cytometry analysis. LX2 monocultures demonstrated a homogenous cell-population according to size (forward-scattered; FSC), granularity and αSMA expressions. However, on their co-culture with NK cells, the HSCs formed four subpopulations, which were stratified by αSMA intensities and cell size. NK cells isolated from heathy donors did not activate LX2-cells. In contrast, HCV exposed to NK cells from both F1 and F4 fibrosis grade patients, showed elevated CD107a and INF-γ levels and increased αSMA intensities in two of the four cell populations, with fibrosis scoring showing a linear correlation with αSMA intensities and NK phagocytosis. The $\alpha SMA^{intermediate}/Size^{Low}$ HSCs sub-population showed higher proliferation following F4-NK cells with higher phagocytosis ability, suggesting an active/regulatory population. The $\alpha SMA^{high}/Size^{high}$ subpopulations showed low proliferation and phagocytosis capacity, and were correlated with higher apoptosis, increased ROS and P15 intensities, suggesting senescing cells. Taken together, NK cells lead to heterogeneous differentiation of HSCs. Flow-cytometry may provide a novel means of characterizing HSCs in relation to the severity of liver fibrosis. © 2018 International Society for Advancement of Cytometry

Key terms

NK cells; hepatic stellate cells; liver fibrosis; flow cytometry

Hepatic fibrosis is a wound healing response to chronic liver injury of various etiologies (1). Activation of hepatic stellate cells (HSCs) and their transdifferentiation to myofibroblasts, the major extracellular matrix-producing cell in fibrotic liver, represents a critical step in the path to fibrosis (1). Typically, cell death of hepatocytes creates an inflammatory microenvironment, which activates HSCs (2,3). Key factors driving HSC activation are transforming growth factor beta 1 (TGF β1) and platelet-derived growth factor (PDGF) family members (4). Moreover, numerous cytokines and chemokines released by infiltrating immune cells modify this process (5,6).

Although lymphocytes directly interact with HSCs by adhesion (7), the pathways mediating lymphocyte-HSCs interactions are not well-understood. We previously showed that CD8 lymphocyte-subsets mediate hepatic fibrosis (8). In states of liver injury, natural killer (NK) cells become stimulated, as manifested by decreased

ISAC
International Society for Advancement of Cytometry

expression of inhibitory killing immunoglobulin receptors, in comparison to the activation receptors. Conversely, HSCs activation, leads to reduced expression of class I molecules, leading NK cells to recognize HSCs as "non-self," which, in turn, provokes HSCs killing (9–12).

In general, HSCs activation in response to hepatocyte damage results in changes that increase NK cell stimulation and decrease their inhibition. Here, we hypothesized that HSCs differentiation to alpha-smooth muscle actin (αSMA)-positive myofibroblasts is regulated by NK cells of different severities of fibrosis. In addition, this work describes the development of a flow cytometry technique for categorization of HSCs into four different groups, each representing a different degree of liver fibrosis. The flow cytometry technique could be used as a tool to study liver microenvironment through the in vitro interplay between cells and evaluate phenotype changes that could be of prognostic value.

Patients and Methods

Study Population

Blood samples of chronic HCV patients referred for liver biopsy (Table 1) were obtained with informed consent, after approval of the Hadassah Hospital Ethics Committee. All HCV patients were positive for serum HCV antibodies (Abbot) and HCV RNA (tested by HCV Amplicor, Roche). Advanced fibrosis was clinically established by the presence of splenomegaly, thrombocytopenia, and irregular liver echotexture, and confirmed by liver biopsy demonstrating Metavir F3 or F4, as assessed by a single pathologist. No patient had evidence of HBV/HCV, HBV/human immunodeficiency virus or HCV/human immunodeficiency virus co-infection.

Lymphocytes and NK Isolation

Human peripheral blood lymphocytes from patients and healthy volunteers were collected in heparinized tubes. Mononuclear cells were isolated by centrifugation over Ficoll-Hypaque (Pharmacia). After three washes in saline, cells were resuspended in medium. NK were further isolated using a magnetic cell sorting kit (Miltenyi Biotec), according to the manufacturer's instructions.

In Vitro Analysis of Human NK Cell Interactions with HSCs

LX2 (10^5 cells), a human HSC line, were cultured for 3 days, up to semi-confluence. Quiescent activation was achieved when LX2 cells were cultured in DMEM medium with 1% fetal bovine serum (FBS), in 6-well flasks (Nunc Brand Products, Denmark) for 24 h. Cells were then co-cultured with healthy or HCV-derived NK cells (10^6 cells), collected from patients with different fibrosis scores ($n = 8$ per fibrosis score). Co-incubations were performed in 18-mm dishes, in 1% FBS (Atlantic Biologicals) medium containing 1% glutamine and streptomycin (Biological industries, Israel). Three cultures were prepared from each NK cell donor. After 24 h of co-culture, medium with unattached NK cells were removed, and cells were trypsinized (0.05% trypsin/0.53 mM EDTA) washed and analyzed for αSMA and NK phagocytosis by flow cytometry.

Table 1. Population characteristics

	HEALTHY	HCV
Number	9	27
Female	3	15
Age (years)	35.8 ± 7	42.9 ± 15
ALT (Units)* 7–55 units	23.5 ± 4	106 ± 98
Albumin* 35–55 g/liter.	41.5 ± 4.6	36.1 ± 4.2
Platelets* 150,000–450,000/dl	320 ± 81	119 ± 41
F- score (n)	Metavir scale None	Metavir scale
F1		9
F2		7
F3		6
F4		6
HCV Genotype 1		23
HCV Genotype 2		1
HCV Genotype 2		2
HCV Genotype 4		1

*Mean + *normal ranges*.

Characteristics of HCV patients. Advanced fibrosis was clinically established by the presence of splenomegaly, thrombocytopenia, elevated serum ALT levels, low ranges of serum albumin and irregular liver echotexture, and confirmed by liver biopsy demonstrating Metavir F3 or F4, as assessed by a single pathologist. No patient had evidence of HBV/HCV, HBV/human immunodeficiency virus or HCV/human immunodeficiency virus co-infection.

Proliferation Assay

Cultured LX2 cells were washed following harvesting and stained with 5,6-carboxyfluorescein diacetate (CFSE), according to the manufacturer's protocol (Invitrogen, Oregon). Briefly, CFSE staining of LX2 after labeling is extremely high intensity fluorescence. The majority of CFSE initially taken up by the cells is lost within the first few days following proliferation. The greater the decrease in fluorescence, the greater the number of cell doublings. Results were obtained as mean fluorescence intensity (MFI- arbitrary unit) and were calculated to fold change in Day 2 as compared to day Zero.

Flow Cytometry Analysis

Harvested LX2, LX2/NK co-cultured cells and isolated NK cells were adjusted to 10^6/ml in staining buffer (diluted in saline containing 1% bovine albumin; Biological Industries, Israel). To determine HSC activation, LX2 cells were fixed with 4% paraformaldehyde for 10 min and permeabilized with 0.1% saponine in PBS for 20 min, then stained with intracellular anti-human αSMA-PE monoclonal-antibody (R&D systems, Minneapolis, MN) or anti-human glial fibrillary acidic protein (GFAP)-Alexa Fluor 488 monoclonal-antibody (eBioscience™, MA, USA) for 30 min at room-temperature. Human NK cells were stained with the pan-leukocytes marker anti-CD45 (Per-CP) (IQ Products, Groningen; diluted 1:40). In addition, the T cell marker anti-CD3

(APC) and the NK marker anti-CD56 (FITC) (IQ Products, Groningen) were used to exclude NKT cells. In each set of experiments, unstained controls, IgG isotype controls as well as fluorescence-minus-one (FMO) controls were prepared. For apoptosis and viability measurements, propidium-iodide (PI) staining of fragmented DNA and phosphatidylserine staining by FITC-conjugated annexin V (R&D Systems) were performed according to the manufacturer's instructions. Apoptosis was defined as annexin-V (+) and PI (–) cells. Viable cells were defined as annexin-V (-) and PI (–) cells. Phagocytosis was defined as CD3- CD56+ and αSMA+ cells simultaneously gating for both NK cells and LX2.

To detect INF-γ and anti-INK4b (p15) expression, HSCs were fixed with 4% paraformaldehyde for 10 min and permeabilized with 0.1% saponine for 20 min. Intracellular staining was performed with anti-INF-γ antibodies (IQ Products, Groningen) or mouse monoclonal anti-INK4b (p15) antibody (EMD Millipore). In both cases, APC-conjugated mouse anti-human antibodies were used as secondary antibodies. To determine oxidative stress, a reactive oxygen species (ROS) assay were performed. Briefly, co-cultured cells were incubated with 100 μmol/l (final concentration) 2′-7′-dichlorofluorescin diacetate (DCF) (Sigma) for 15 min, at 37°C, in a humidified atmosphere of 5% CO_2 in air. The cells were washed twice, resuspended in PBS and analyzed with a flow cytometer (Becton-Dickinson LSR II, Immunofluorometry Systems, Mountain View, CA).

Immunofluorescence Staining

Liver biopsy samples were incubated overnight at room temperature, in isotonic PBS, 10% sucrose, and 4% formaldehyde solution. Samples were then embedded in Optimal cutting temperature compound, and then frozen at−20°C for 24 h prior to storage at −80°C. Seven μm-thick frozen sections were prepared using a Cryostat (Leica CM 3000). After 20 min incubation in 1% bovine serum albumin and PBS washing, slides were incubated with primary antibody for 45 min at room temperature, in the dark. To identify HSCs, samples were incubated with anti-αSMA antibody (DAKO, cat# M0851; 1:150), and later with Cy5-conjugated antibody (Jackson Immunoresearch; 1:40). To preserve staining, sections were covered with Fluoromount-G (Southern Biotechnology Associates) and then stored at 4°C until analysis.

Confocal Microscopy and Image Capture

A Zeiss LSM 410 Confocal laser scanning system (Zeiss, Germany), attached to a Zeiss Axiovert 135 M microscope, with plan-apochromat Zeiss 40 X 1.4 lenses, was used to analyze tissue and cell samples. The system was equipped with helium-neon lasers (543 nm and 633 nm lines). In each experiment, laser intensity, background level, contrast, aperture, and electronic zoom size were collected at the same level. Fifty images were collected from each specimen and converted to tiff format and processed using Zeiss LSM Image Browser software.

Image processing was performed using Adobe Photoshop software (Adobe Systems UK, Uxbridge, and Middlesex, UK) and ImagePro Plus programs (Media Cybernatics).

Statistical Methods

Results are presented as mean ± standard deviation. For statistically significant differences, paired and unpaired Student's t test and analysis of variance were used. In addition, the repeated measures mixed-design model was utilized. This was followed by Bonferroni test, in order to adjust for multiple comparisons and to control Type I error.

Results

Characterization of Four Subtypes of HSCs in Relation to Liver Fibrosis Severity

We have previously shown (7) that NK cells derived either from healthy or from patients with HCV adhere to LX2 and eventually phagocytose inside the LX2. Flow cytometry could be a beneficial tool for studying cells in cultures and their phenotype alterations and could be used as predictive tool for fibrosis severities. Therefore, we aimed to harness flow cytometry to test the potential of NKs to modulate phagocytosis through its effect on HSCs.

Monocultures of the LX2 human HSC line demonstrated a single homogenous cell population, which could be categorized by size (forward-scattered; FSC) and granularity (side-scattered; SSC) (Fig. 1A). αSMA staining of LX2 cells showed MFI of ∼1,000 arbitrary units (A.U.), with 94% of the population showing αSMA+, indicating a homogenous and active cell population (Fig. 1B). The line in Figure 1B was set according to the LX2 cells stained with the isotype control.

Figure 1C shows a representative dot plot analysis of LX2 following co-culture with NK cells from healthy donor. Gating of both the NK (purple population; purple gate) and LX2 (green population; green gate) were performed according to size and granularity. As LX2 phagocytose NK cells, our gating strategy was based to include all cell populations in our samples as one population, therefore, another gate (red color) was set to include our target populations (live) and to exclude dead populations. Red gating of the results in Figure 1C, yielded four subpopulations differentiated by both αSMA fluorescence intensities as well their size variations (Fig. 1D). The same line plotted in Figure 1B was drawn in Figure 1D to better show the LX2 sub-differentiation. The four LX2 cell subpopulations included: 1-HSCs with low intensity of αSMA, low size ($\alpha SMA^{Low}/Size^{Low}$) (lower left population), 2-HSCs with intermediate intensity of αSMA, low size ($\alpha SMA^{Intermediate}/Size^{Low}$) (Upper left population); 3-HSCs with intermediate intensity of αSMA, high size ($\alpha SMA^{Intermediate}/Size^{High}$) (lower right population), and 4-HSCs with high intensity of αSMA, high size ($\alpha SMA^{High}/Size^{High}$) (Upper right population).

To confirm that these four populations are LX2 subsets, the cells were stained for GFAP, an early HSCs activation marker (13). All LX2 subpopulations showed expressions of GFAP and the fluorescence intensities were linearly associated with high αSMA (Fig. 1E). Figure 1F shows gating strategies set on each of the generated HSCs subpopulations. The gates (G1 to G4) are shown in the figure. Figure 1G shows

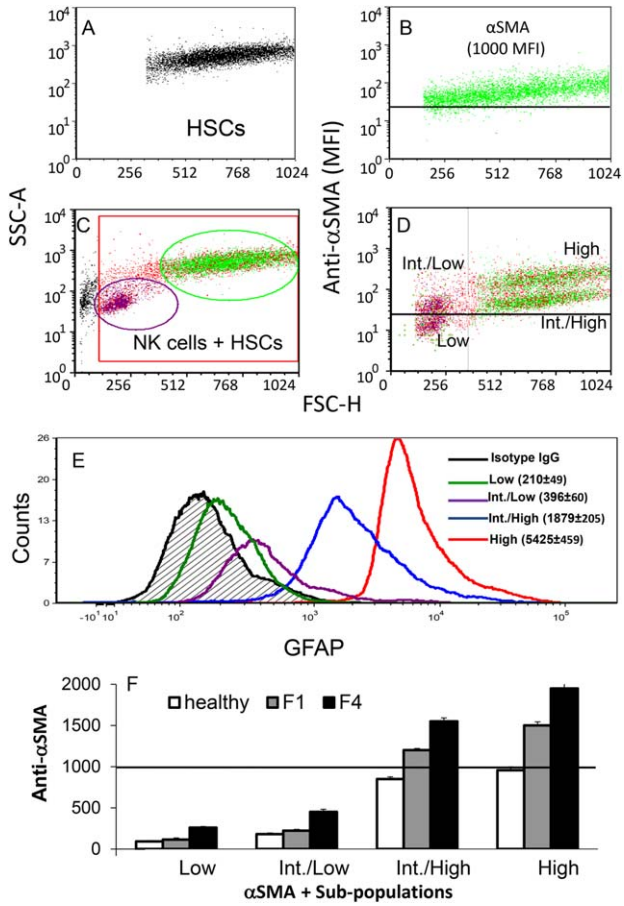

Figure 1. Flow cytometry analysis detected four HSCs subpopulations. LX2 were mono-cultured for 24 h in 10% Fetal Calf Serum and analyzed for (**A**) size (forward-scattered; FSC), granularity and (**B**) αSMA expression (green) (αSMA intensity ~1,000 arbitrary-units). (**C**) A representative dot plot of co-cultures of gated NK cells (purple) with gated LX2 (green), showing two cell populations according to size (forward-scattered; FSC), and granularity. Another gate (red color) was set to include live and exclude dead populations. (**D**) Four αSMA subpopulations differing in their αSMA intensities and size following co-cultures (**E**) Representative flow cytometry histograms of LX-2 cells expressing GFAP. Isotype control of a representative sample from HCV patient with F4 score is displayed in black, and the samples incubated with anti-GFAP-Alexa Fluor 488 are indicated in colored histograms for each of the gated LX2-subpopulations. MFI±SD are presented to each of the tested LX2-subpopulations. (**F**) Shows gating strategies set on each of the generated HSCs subpopulations. The gates (G1 to G4) are shown in the figure. (**G**) Co-culture averages of the gated subpopulations (G1 to G4) of eight patients in each of healthy donors, HCV patients of F1 and F4 scores showing αSMA increased in different subpopulations and in line of fibrosis staging ($P < 0.05$). In each experimental setting, unstained controls as well as IgG isotype controls were used.

the averages of gated αSMA intensities of the different HSCs subpopulations following incubations with NK cells isolated from HCV patients with different fibrosis-scoring (early fibrosis; F1 and advanced fibrosis; F4). When compared to NK cells from healthy donors, in each sub-population a linear correlation between fibrosis-scoring and αSMA-intensities were seen. A line was drawn on the scale of the MFI of 1,000; which are the average results of HSCs monoculture. NK cells from healthy donors inactivated LX2 cells (as compared to LX2 monocultures), as manifested by decreased αSMA intensities, in all the four subpopulations, while NK cells from the HCV patients increased αSMA-intensities in two of the four subpopulations; the $\alpha SMA^{Intermediate}/Size^{High}$ and $\alpha SMA^{High}/Size^{High}$ subpopulations indicating inability of NK cells to reduce fibrosis of high αSMA HSCs.

Liver Biopsy from F4 HCV Patients Showed High αSMA Intensities

Using confocol microscopy, we previously demonstrated direct contact of HCV-derived NK cells with cultured human HSCs (7). To this end, we stained HSCs from liver biopsies of HCV patients with different fibrosis scores. Liver biopsies were incubated overnight at room temperature with isotonic PBS, 10% sucrose, and 4% formaldehyde solution. Then they were frozen at −80°C for storage, and 7-μm-thick frozen sections were prepared using Cryostat (Leica CM 3000). F1 and F2-associated HSCs showed scattered and weak αSMA staining, which gradually became prominent in fibrotic livers of F3 and F4 scores (Fig. 2). Taken together with the flow cytometry results, the $\alpha SMA^{Intermediate}/Size^{High}$ and $\alpha SMA^{High}/Size^{High}$ HSCs are likely those that differentiate and play a role in fibrosis progression.

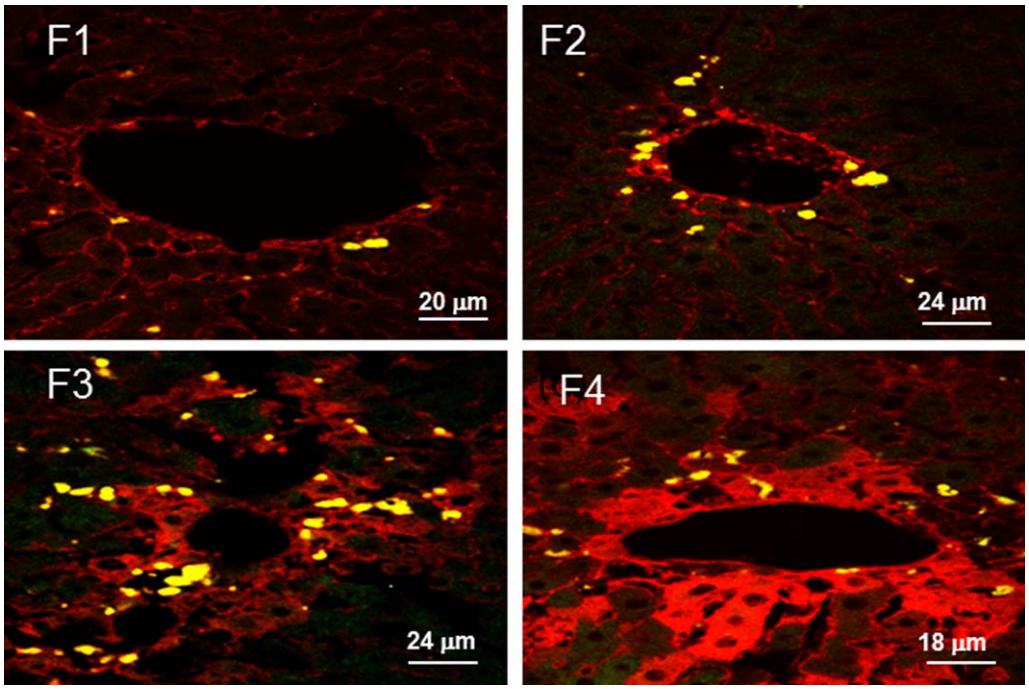

Figure 2. αSMA HSCs levels in liver biopsy samples. Liver biopsies from fibrotic HCV patients (**A–D**) were stained with anti-αSMA antibodies, and then with Cy-5 conjugated secondary antibodies, to detect HSCs. Confocal laser scanning microscopy was used to visualize stained sections.

NK Cells of HCV Patients Induce HSCs Proliferation

To evaluate the impact of NK cells of HSCs proliferation, NK cells obtained from HCV patients with various fibrosis score were co-cultured with LX2, stained for CFSE and subjected to flow cytometry analysis 12 and 48 h following co-cultures. Figure 1F shows HSCs proliferations calculated from the gated populations as fold change in CFSE fluorescence. NK cells from healthy donors induced a prominent increase in proliferation of the two HSCs subpopulations with elevated αSMA fluorescence intensities, and primarily, of the $\alpha SMA^{Intermediate}/Size^{High}$ population (Fig. 3). In parallel, NK cells from HCV patients led to a significant increase in proliferation rates of the $\alpha SMA^{Intermediate}/Size^{Low}$ population, while mild increase in the $\alpha SMA^{Intermediate}/Size^{High}$ and $\alpha SMA^{High}/Size^{High}$ subpopulations, suggesting a functional role of the HSCs subpopulation with intermediate intensities of αSMA in fibrogenesis.

Flow Cytometry Phenotype Evaluation of LX2 Subpopulations

To further characterize these HSCs subpopulations, we set out to determine their ability to phagocytose NK cells, by means of a specially designed flow cytometry technique. A FMO control served to optimize the identification of NK cells and LX2 cells under both monoculture and co-culture conditions. Figures 4A and 4B show dot plot of unstained control, the FMO control and the fully stained cell sample (test stain) stained with anti-CD56–FITC (fluorescein isothiocyanate) and anti-αSMA-PE (phycoerythrin) after compensation. Figure 4C shows the FMO control for co-culture conditions of both NK with LX2 cells. As shown in the FMO control dot plot, the cells were shifted to the right indicated presence of NK cells and an FMO line was set to better indicate negative-control position of LX2 in addition to the unstained line. In the stained sample, around 97% of our LX2 population showed to be positive for αSMA also an indication that the NK cells co-cultured with LX2 were either adhered or phagocytized in LX2.

Figure 4D shows the $\alpha SMA^{Intermediate}/Size^{High}$ subpopulation displayed the highest percentage of phagocytosis (81%) of healthy NK cells, while the $\alpha SMA^{High}/Size^{High}$ subpopulation showed the lowest (13%). In contrast, $\alpha SMA^{Intermediate}/$

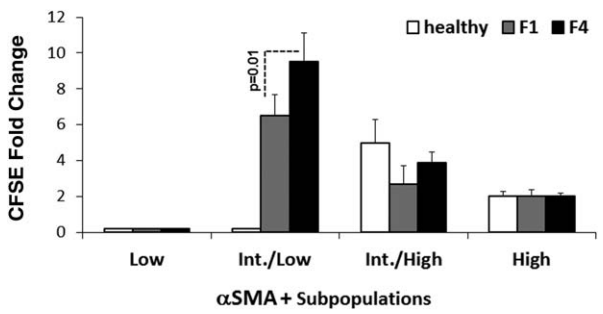

Figure 3. LX2 proliferation rate following in vitro co-culture with NK cells. Adhered LX2 cells after co-culture for 24 h with NK cells from healthy or F1 and F4 fibrosis HCV patients, were analyzed for proliferation by monitoring CFSE levels, using flow cytometry. Proliferation fold changes were calculated by dividing Day 2 readings by Day 0 readings, as described in Materials and Methods.

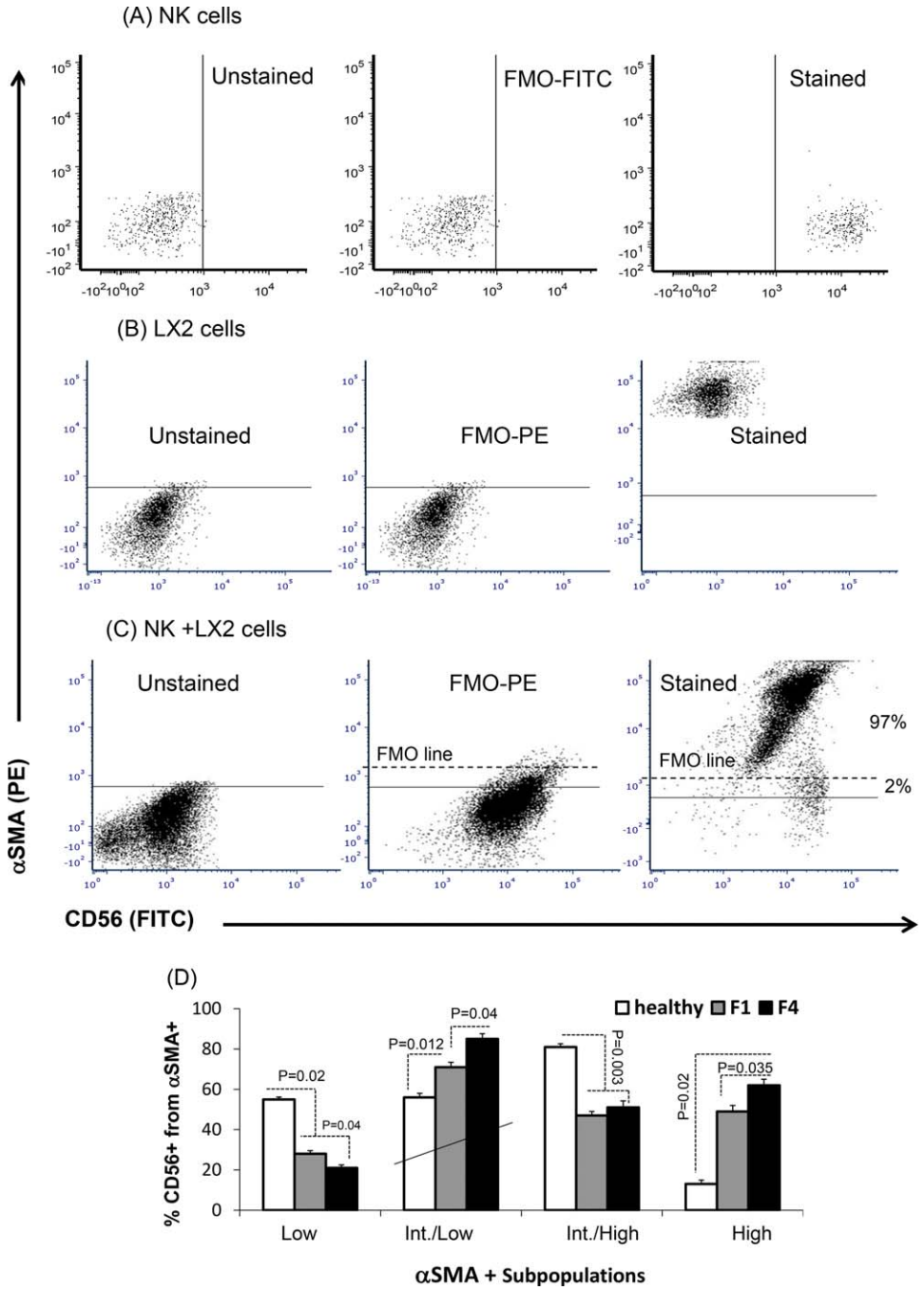

Figure 4. Flow cytometry analysis of phagocytosis of NK cells by LX2. In this sample experiment, a fluorescence-minus-one (FMO) control was devised to optimize the identification of NK cells and LX2 cells. (**A–C**) The unstained control, the FMO control and the fully stained cell sample (test stain) stained with anti-CD56–FITC (fluorescein isothiocyanate) and anti-αSMA-PE (phycoerythrin) are shown after compensation. In (C) shows the FMO control for co-culture conditions of both NK and LX2 cells. An FMO line was set to better indicate negative-control position of LX2 in addition to the unstained line. Around 97% of our population showed positive for αSMA. (**D**) Phagocytosis was defined as CD56+ from αSMA+ gating's of LX2. $\alpha SMA^{Intermediate}/Size^{High}$ subpopulations phagocytized more of the NK cells obtained from the healthy donors (white bars; $P = 0.02$), $\alpha SMA^{Intermediate}/Size^{Low}$ phagocytized NK cells obtained from the HCV patients with a graduate increase of the F4 cells (Black bars; $P = 0.04$). The $\alpha SMA^{Intermediate}/Size^{Low}$ subpopulations showed phagocytosis correlated with *F* score. [Color figure can be viewed at wileyonlinelibrary.com]

$Size^{Low}$ HSCs isolated from F1 (gray bars) and F4 (black bars) fibrosis patients showed the greatest extent of NK cell phagocytosis as compared to the other subpopulations. Also, these subpopulations had similar high proliferation rates following incubations with NK cells of HCV patients. The $\alpha SMA^{Intermediate}/Size^{Low}$ sub-populations shows a linear fibrosis scoring compatible with the NK from healthy and HCV donors of both F1 and F4 grades.

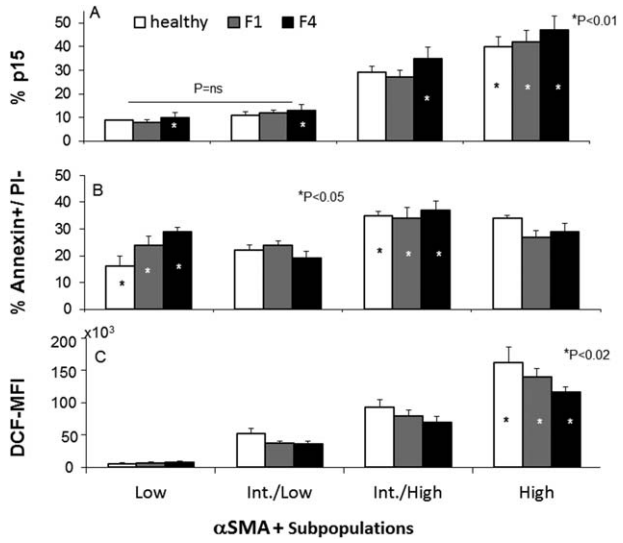

Figure 5. Flow cytometry measurement of senescence, apoptosis and oxidative stress in the LX2 $\alpha SMA^{high}/Size^{high}$ subpopulation. (**A**) Senescence of LX2 cells, defined as αSMA + P15+. (**B**) Apoptotic LX2 cells, defined as αSMA + Annexin+ and PI–. (**C**) LX2 ROS productions, defined as αSMA + DCF+.

The above findings confirm the importance of the intermediate αSMA populations in modulating fibrosis severity and correlate high αSMA intensities with low phagocytosis, possibly due to aging induced on full differentiation.

Krizhanovsky et al. (14) showed that senescence of activated HSCs limits the extent of fibrosis following liver damage, underscoring the interplay between senescent cells and the tissue microenvironment. To evaluate senescence in each of the HSC subpopulations, cells were stained for the senescence marker, p15, a cyclin-dependent kinase inhibitor (CDKI). Elevated p15 expression was observed in both the large-sized intermediate and highly expressing αSMA populations following their incubation with NK cells from healthy donors or from F1 or F4 HCV patients (Fig. 5A). p15 expressions in $\alpha SMA^{High}/Size^{High}$ populations showed a linear correlation with fibrosis scores, with cells isolated from F4 patients showing the highest expression of p15 (47%; $P = 0.01$) $\alpha SMA^{Intermediate}/Size^{High}$ from F4 patients showed 29% expression, while $\alpha SMA^{Intermediate}/Size^{Low}$ and $\alpha SMA^{Low}/Size^{Low}$ subpopulations showed low p15 expressions of 12% and 10%, respectively.

We next sought to determine whether differences in HSCs proliferation rates and senescence correlate with both apoptosis rates and generation of ROS, which may contribute to changes in αSMA intensities. Krizhanovsky et al. suggested that in addition to halting proliferation, senescent cells can also display dramatic changes in their secretory properties (14). For example, senescent cells down regulate genes encoding extracellular matrix components and up regulate extracellular matrix-degrading enzymes (e.g., matrix metalloproteinases), although the biological consequences of these effects have not been considered. Apoptosis of HSCs, defined as Annexin V+/PI– cells, was elevated in $\alpha SMA^{Intermediate}/Size^{High}$ and $\alpha SMA^{High}/Size^{High}$ as compared to the αSMA^{low} populations (Fig. 5B; $P < 0.05$). In parallel, both $\alpha SMA^{Intermediate}/Size^{High}$ and $\alpha SMA^{High}/Size^{High}$ subpopulations displayed elevated levels of ROS (Fig. 5C). These results were well correlated with high expressions of P15 and apoptotic rate in the $\alpha SMA^{High}/Size^{High}$ subpopulations indicating their approach to death destiny. These findings suggest a regulative role of the other HSCs subpopulations in fibrogenesis, via both physical interaction with NK cells and active clearance of NK clearance cells via phagocytosis.

Flow Cytometry Phenotype Evaluation of NK Cells

To determine whether changes in HSCs phenotypic relate to NK cell activity, NK cells were evaluated immediately following isolation from HCV fibrosis patients, for NK cell activity marker CD107a (lysosomal-associated membrane protein 1 (LAMP-1)) (15) expression and for their INF-γ-secreting potential. Figure 6 shows a significant decrease in both CD107a as well as in INF-γ in patients with both F1 and F4 fibrosis score. These reductions in their activity were correlated with fibrosis severity. The results suggest changes in HSCs phenotype in fibrosis patients with HCV could be directly affected whether NK cells are active or not and therefore focus on NK cells as potential targets to control fibrogenesis.

Discussion

The current study assessed the possible role of flow cytometry as a non-invasive technique for fibrosis scoring. The study of HSCs may provide important mechanistic insights into the pathophysiology of liver fibrosis and may hold the key to development of effective means of blocking their activation and therefore inhibit liver fibrosis. In this work, we used the LX-2 cell line, which may constitute a good model of human HSCs and can thus avoid the need for human primary cells in research (16,17) LX-2 cells express αSMA, vitamin A, the intermediate filament protein GFAP, and the type β receptor for PDGF, suggesting that the cells line retains key features of activated/transdifferentiated HSCs. In pharmacological studies, Ghazwani et al. showed that LX-2 cells have the same physiological responses as primary HSCs (18).

In recent years, it has become clear that HSCs are prominent determinants of hepatic immunoregulation during injury. The cells express a battery of chemokines (including CCL2, CCL5, CXCL2, CXCL8, CXCL9, CXCL10, CXCL12, and CX3CL3) known to recruit neutrophils, macrophages/monocytes, NK cells, dendritic cells, NK T cells, and other T cells (19,20). Furthermore, activated HSCs secrete inflammatory mediators in response to signals such as TNF-α, IL-1beta, and lipopolysaccharide. Hence, HSCs amplify the inflammatory response in the context of liver disease (21).

In our pursuit of anti-fibrosis strategies, including inhibition of HSC activation and induction of HSC apoptosis, we studied HSCs/lymphocytes interactions and showed that as opposed to CD8+ immune cells, NK cells display anti-fibrotic

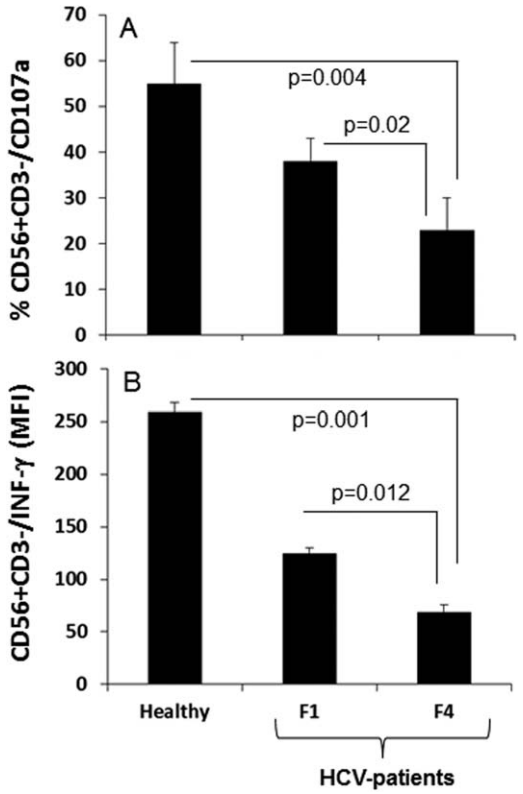

Figure 6. NK from HCV patients had low activity. NK cells isolated form different fibrosis stages showed (**A**) decreased in their CD107a and (**B**) decreased in their INF-g levels as compared to their normal counterparts. The decrease in NK activity was correlated with the increase in the fibrosis score ($P < 0.05$).

activity through stimulation of HSCs killing (7,10,11). Function impairment of NK cells was explored as a possible mechanism for fibrosis progression into cirrhosis.

In the current study, we adapted a previously described co-culture assay (22), in which HSCs are cultured with peripheral blood NK cell. Flow cytometry and confocal microscopy were used to evaluate interactions between NK cells and HSCs in in vitro and in situ contexts, respectively. We showed that NK cells, whether HCV-infected or uninfected, induced in vitro HSC differentiation into subpopulations that differ in their αSMA expression and sizes. NK cells from healthy donors deactivated HSCs, which correlated with decreased αSMA intensities in all subpopulations. In parallel, NK cells from low fibrosis (F1) and high fibrosis (F4) patients deactivated HSCs within two subpopulations of small-sized cells with either low or intermediate αSMA expression ($\alpha SMA^{Low}/Size^{Low}$, $\alpha SMA^{Intermediate}/Size^{Low}$). In contrast, they were associated with large-sized HSCs displaying high αSMA expression ($\alpha SMA^{Intermediate}/Size^{High}$, $\alpha SMA^{High}/Size^{High}$).

The $\alpha SMA^{Intermediate}/Size^{Low}$ subpopulation showed increased phagocytosis of NK cells of F1 and F4 fibrosis grade patients, as compared to the other HSCs subpopulations. This population also showed higher proliferation rates following incubations with NK cells of HCV patients. These findings confirm the importance of the intermediate αSMA-expressing populations in modulating fibrosis destiny. The low phagocytosis potentials of populations expressing high αSMA levels, raises the possibility of the shift to aging processes on full differentiation. Thus, we assessed the apoptosis rate and ROS levels, both hallmarks of senescence, in HSCs subpopulations.

ROS and other oxidative stress-related intermediates contribute to death, the perpetuation of chronic inflammatory responses and fibrogenesis, particularly, hepatic chronic wound healing and liver fibrogenesis (23,24). ROS are involved in necrosis and apoptosis of hepatocytes and consequential HSCs activation (25) Indeed, our results showed elevated levels of ROS in the highly activated HSCs of both $\alpha SMA^{Intermediate}/Size^{High}$ and $\alpha SMA^{High}/Size^{High}$ subpopulations. Conversely, senescent cells display a large, flattened morphology and senescence-associated β-galactosidase (SA-β-gal) activity that distinguishes them from most quiescent cells (26) In addition, they often downregulate genes involved in proliferation and extracellular matrix production and upregulate inflammatory cytokines and other molecules known to modulate the microenvironment or immune response (26,27) Furthermore, senescent HSCs express reduced levels of extracellular matrix proteins, including collagens, tenascin, and fibronectin (27) TUNEL staining of senescent HSCs showed approximately 21% positive cells, indicating DNA fragmentation and apoptosis (26). In agreement, our flow cytometry analysis of HSCs showed elevated expressions of P15 in both $\alpha SMA^{Intermediate}/Size^{High}$ and $\alpha SMA^{High}/Size^{High}$ correlated with the HSCs subpopulations of high αSMA activations.

HSCs phagocytosis of NK cells is a newly discovered and potentially important pathway in regulation of the impact of HSCs on the course of hepatic fibrosis. Our study suggests that flow cytometry could serve as a novel tool to study differentiation of HSCs populations and to score fibrosis, especially when only 1/50,000 of the whole liver tissue is sampled during a liver biopsy, for which sampling error is of concern. As peripheral lymphocytes contribute to variant HSCs differentiation, we propose the described populations as a basis for development of an assay for prediction and personalization of anti-fibrotic therapies.

Literature Cited

1. Yin C, Evason KJ, Asahina K, Stainier DY. Hepatic stellate cells in liver development, regeneration, and cancer. J Clin Invest 2013;123:1902–1910.
2. Tu T, Calabro SR, Lee A, Maczurek AE, Budzinska MA, Warner FJ, McLennan SV, Shackel NA. Hepatocytes in liver injury: Victim, bystander, or accomplice in progressive fibrosis? J Gastroenterol Hepatol 2015;30(12):1696–1704.
3. Coulouarn C, Corlu A, Glaise D, Guénon I, Thorgeirsson SS, Clément B. Hepatocyte-stellate cell cross-talk in the liver engenders a permissive inflammatory microenvironment that drives progression in hepatocellular carcinoma. Cancer Res 2012; 72(10):2533–2542.
4. Liu C, Li J, Xiang X, Guo L, Tu K, Liu Q, Shah VH, Kang N. PDGF receptor-α promotes TGF-ß signaling in hepatic stellate cells via transcriptional and posttranscriptional regulation of TGF-ß receptors. Am J Physiol Gastrointest Liver Physiol 2014; 307(7):G749–G759.
5. Marra F, Tacke F. Roles for chemokines in liver disease. Gastroenterology 2014; 147(3):577–594.
6. Cubero FJ. Shutting off inflammation: A novel switch on hepatic stellate cells. Hepatology 2016;63(4):1086–1089.
7. Muhanna N, Doron S, Wald O, Horani A, Eid A, Pappo O, Friedman SL, Safadi R. Activation of hepatic stellate cells after phagocytosis of lymphocytes: A novel pathway of fibrogenesis. Hepatology 2008;48(3):963–977.

8. Vinas O, Bataller R, Sancho-Bru P, Gines P, Berenguer C, Enrich C, Nicolás JM, Ercilla G, Gallart T, Vives J, et al. Human hepatic stellate cells show features of antigen-presenting cells and stimulate lymphocyte proliferation. Hepatology 2003; 38:919–929.
9. Safadi R, Ohta M, Alvarez CE, Fiel I, Bansal M, Mehal W, Friedman SL. Immune stimulation of hepatic fibrogenesis by CD8 lymphocytes and its attenuation by transgenic interleukin 10 from hepatocytes. Gastroenterology 2004;127:870–882.
10. Melhem A, Muhanna N, Bishara A, Alvarez CE, Ilan Y, Bishara T, Horani A, Nassar M, Friedman SL, Safadi R. Anti-fibrotic activity of NK cells in experimental liver injury through killing of activated HSC. J Hepatol 2006;45:60–71.
11. Radaeva S, Sun R, Jaruga B, Nguyen VT, Tian Z, Gao B. Natural killer cells ameliorate liver fibrosis by killing activated stellate cells in NKG2D–dependent and tumor necrosis factor-related apoptosis-inducing ligand-dependent manners. Gastroenterology 2006;130:435–452.
12. Muhanna N, Horani A, Doron S, Safadi R. Lymphocyte-hepatic stellate cell proximity suggests a direct interaction. Clin Exp Immunol 2007;148:338–347.
13. Carotti S, Morini S, Corradini SG, Burza MA, Molinaro A, Carpino G, Merli M, De Santis A, Muda AO, Rossi M, et al. Glial fibrillary acidic protein as an early marker of hepatic stellate cell activation in chronic and posttransplant recurrent hepatitis C. Liver Transplantation 2008;14:806–814.
14. Krizhanovsky V, Yon M, Dickins RA, Hearn S, Simon J, Miething C, Yee H, Zender L, Lowe SW. Senescence of activated stellate cells limits liver fibrosis. Cell 2008; 134(4):657–667.
15. Alter G, Malenfant JM, Altfeld M. CD107a as a functional marker for the identification of natural killer cell activity. J Immunol Methods 2004;294:15e22.
16. Xu L, Hui AY, Albanis E, Arthur MJ, O'Byrne SM, Blaner WS, Mukherjee P, Friedman SL, Eng FJ. Human hepatic stellate cell lines, LX-1 and LX-2: New tools for analysis of hepatic fibrosis. Gut 2005;54:142–151.
17. Robert S, Gicquel T, Bodin A, Lagente V, Boichot E. Characterization of the MMP/TIMP imbalance and collagen production induced by IL-1β or TNF-α release from human hepatic stellate cells. PLoS One 2016;11(4):e0153118.
18. Ghazwani M, Zhang Y, Gao X, Fan J, Li J, Li S. Anti-fibrotic effect of thymoquinone on hepatic stellate cells. Phytomed Int J Phytother Phytopharm 2014;21:254–260.
19. Panebianco C, Oben JA, Vinciguerra M, Pazienza V. Senescence in hepatic stellate cells as a mechanism of liver fibrosis reversal: A putative synergy between retinoic acid and PPAR-gamma signalings. Clin Exp Med 2017;17:269–280.
20. Matsuoka M, Tsukamoto H. Stimulation of hepatic lipocyte collagen production by Kupffer cell-derived transforming growth factor beta: Implication for a pathogenetic role in alcoholic liver fibrogenesis. Hepatol Baltim Md 1990;11:599–605.
21. Friedman SL. Hepatic stellate cells: Protean, multifunctional, and enigmatic cells of the liver. Physiol Rev 2008;88:125–172.
22. Abu-Tair L, Doron S, Mahamid M, Amer J, Safadi R. Leptin modulates lymphocytes' adherence to hepatic stellate cells is associated with oxidative status alterations. Mitochondrion 2013;13(5):473–480.
23. Pinzani M, Marra F. Cytokine receptors and signaling in hepatic stellate cells. Semin Liver Dis 2001;21:397–416.
24. Panth N, Paudel KR, Parajuli K. Reactive oxygen species: A key hallmark of cardiovascular disease. Adv Med 2016;2016:9152732.
25. Richter K, Kietzmann T. Reactive oxygen species and fibrosis: Further evidence of a significant liaison. Cell Tissue Res 2016;365(3):591–605.
26. Campisi J, d'Adda di Fagagna F. Cellular senescence: When bad things happen to good cells. Nat Rev Mol Cell Biol 2007;8(9):729–740.
27. Schnabl B, Purbeck CA, Choi YH, Hagedorn CH, Brenner D. Replicative senescence of activated human hepatic stellate cells is accompanied by a pronounced inflammatory but less fibrogenic phenotype. Hepatology 2003;37(3):653–664.